AIAA 81-0708R

Large Inductive Thruster Performance Measurement

R. H. Lovberg*
University of California at San Diego, La Jolla, Calif.
and
C. L. Dailey†
TRW Defense and Space Systems Group, Redondo Beach, Calif.

A 1 m pulsed inductive thruster employing puff-injected argon as a propellant has been constructed and operated in a single-shot mode for measurements of total impulse. I_{sp} and efficiency are then inferred by the combined impulse and total injected mass. Indicated efficiencies are 42% at 1540 s I_{sp} and 50% at 2240 s I_{sp}.

Nomenclature

a = inner radius of coil, m
b = outer radius of coil, m
B, B_r = radial magnetic field, T
C = capacitance of storage bank, F
E_θ = azimuthal electric field, V/m
F_z = axial force, N
g = acceleration of gravity, m/s^2
I_1 = circuit current, A
I_2 = plasma current, A
I_{sp} = specific impulse, s
j_θ = plasma current density, A/m^2
j_s = surface current density, A/m^2
L = circuit inductance, H
L_e = external (parasitic) inductance, H
L_i = initial circuit inductance, H
L_0 = coil inductance unloaded, H
ℓ = stroke length, m
M = mutual inductance, H
m = plasma mass, kg
m_0 = total injected mass, kg
P = power, W
R = resistance per square of plasma, Ω
r = radial coordinate, cm
R_e = external circuit resistance, Ω
R_m = magnetic Reynolds number
R_p = resistance of plasma loop, Ω
t = time, s
t_0 = time equivalent of δ_0, s
T_e = electron temperature, eV
U_R = energy loss to plasma resistance, J
U_p = work done on plasma, J
v = plasma velocity, m/s
V_0 = initial capacitor voltage, V
z = axial coordinate, cm
Z = axial position of current, m
Z_0 = decoupling distance of plasma, m
ΔI = impulse per discharge, N·s
ΔL = change in circuit inductance, H
θ = azimuthal coordinate, deg
δ = thickness of current sheet, m
δZ = depth of initial gas layer, m
δ_0 = initial thickness of current sheet, m
η = efficiency of thruster
η_R = efficiency, resistance limited
ρ_e = electrical resistivity of plasma, Ω·m
ρ_m = axial mass density, kg/m

Presented as Paper 81-0708 at the AIAA/JSASS/DGLR 15th International Electric Propulsion Conference, Las Vegas, Nev., April 21-23, 1981; submitted April 30, 1981; revision received Sept. 23, 1981. Released to AIAA to publish in all forms.

*Professor of Physics.

†Member of Technical Staff.

Introduction

THIS paper reports the experimental results of an investigation of impulse and thrust efficiency of a large-diameter pulsed inductive plasma accelerator. This is a continuation of an ongoing program in which smaller devices of the same kind have previously been studied and generally found to have efficiencies in the range of 5% (20 cm coil, 1200 s I_{sp}) to 18% (30 cm coil, 1470 s I_{sp}).[1,2]

Recent interest in high-thrust, high-power applications led to the consideration of physically larger coils which appear attractive since efficiency has been found to increase with size. In this work we have studied the efficiency scaling theoretically and have constructed and measured the properties of a 1-m-diam coil. We have found a substantial efficiency advantage in the large size.

Elements of the System

The impulsive, inductive acceleration of plasma is conceptually a very simple process, as idealized in Fig. 1. A strong, short pulse of current is sent through a flat annular coil from a low-inductance capacitor bank. A layer of gas, transiently applied to the surface of the coil, is made to break down electrically by the induced azimuthal electric field and the resulting plasma current ring is repelled away from the coil by, as one wishes to view it, a $\boldsymbol{j}\times\boldsymbol{B}$ force arising from interaction between the radial magnetic field and the plasma current or by the mutual repulsion of the two oppositely flowing current rings (plasma and coil).

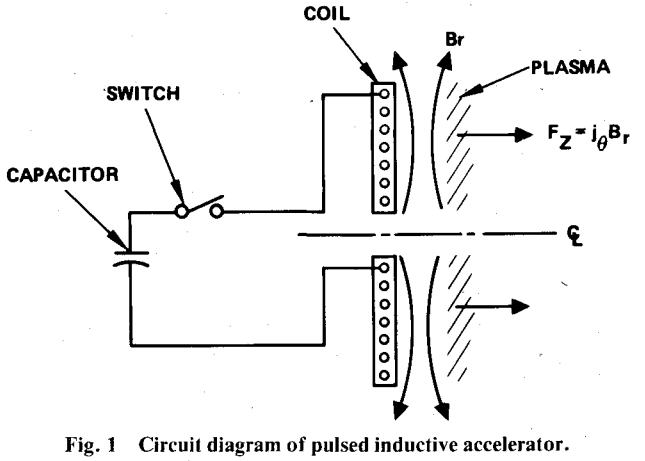

Fig. 1 Circuit diagram of pulsed inductive accelerator.

Simplicity disappears from the problem, however, when one seeks to maximize the energy efficiency of the accelerator. Motion of the plasma ring away from the coil rapidly decouples the two current rings. System design must provide that most of the stored energy be transferred to plasma motion before this decoupling occurs. Unavoidable energy losses occur in the electrical resistance of the coil circuit and plasma, with the latter being the most serious.

An easily derived theorem shows also that the efficiency of a pulsed accelerator, either inductive or series connected, cannot exceed the fractional increase in driving circuit inductance during the stroke, i.e.,

$$\eta < \Delta L/L_i$$

where L_i is the initial circuit inductance and η the efficiency.[3] Parasitic inductance in the circuit must therefore be rigorously minimized.

Finally, nonpropulsive energy losses occur if the body of plasma is not accelerated uniformly as a rigid body.[4] In the "snowplow" limit where the $\boldsymbol{j}\times\boldsymbol{B}$ force is applied to a thin layer at the rear of the plasma, half of the work done by the field goes into the internal, rather than translational, energy of the propellant.

Inductive acceleration has the particular advantage, however, that the electrode losses always incurred in series-connected plasma accelerators (coaxial or rail guns, MPD arcs, etc.) are entirely absent. Since the plasma is lifted away from the coil surface early in the current pulse, conductive transfer of plasma heat to the accelerator structure is small, as is erosion. The only important channel through which energy lost to plasma resistivity can be returned to the accelerator and spacecraft is radiation, and this is always delivered with a smooth nonlocal distribution that minimizes damage. It is possible, moreover, that one may design the surfaces of structures to reflect some substantial fraction of this radiant energy.

Plasma Resistance Losses and Scaling

When the induced electric field E_θ is applied to the propellant gas at the time of circuit switch closure, breakdown follows quickly, i.e., in a time much shorter than the coil current onset time. However, the breakdown interval is not negligibly small, and during this time the conductivity of the plasma swings from zero upward to a value set by the radiatively limited electron temperature. As a result, the initial current sheet thickness in the plasma is somewhat greater than it would be if governed by diffusion at the final T_e.

To simplify discussion of the resistance problem, we consider the one-dimensional situation of Fig. 2. Assume that at $t=0$, the plasma current sheet has a thickness δ_0 imparted to it at breakdown. It is accelerated rightward by a constant B and thickens to a δ by classical diffusion as it moves. Acceleration terminates at some distance ℓ from the surface of origin. This represents the decoupling distance for the annular coil accelerator and, since it is proportional to coil diameter, it may be taken as a linear scaling parameter for the system.

For unit current sheet area, resistive power is $P=j_s^2R$, where $j_s=B/\mu_0$, $R=\rho_e/\delta$, and $\rho_e=$ resistivity.

For classical diffusion,

$$\delta=\sqrt{\rho_e t/\mu_0}$$

where t is time since the switch-on of B to the conductor surface. It will be convenient to account for our starting δ_0 by shifting the origin of time, so that acceleration starts at

$$t_0=\mu_0\delta_0^2/\rho_e$$

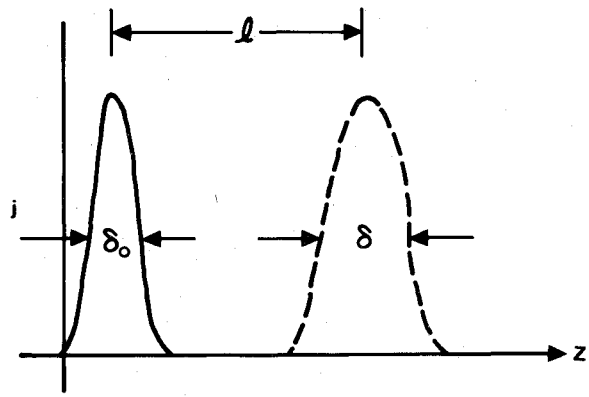

Fig. 2 Thickening of resistive current sheet with increasing time.

Then,

$$P=j_s^2R=\frac{B^2\rho_e}{\mu_0^2\delta}=\frac{B^2\rho_e^{1/2}t^{-1/2}}{\mu_0^{3/2}} \tag{1}$$

For the case of the heavy-ion plasmas employed for propulsion, it is a convenient and quite accurate approximation to assume that resistivity is constant throughout the cycle. The availability of higher ionization states at higher temperatures, with radiation power dependent on the ionic charge squared, tends to strongly "thermostat" electron temperature, so that for argon, as an example, T_e is within half a volt of 3 eV for current densities that differ by more than three orders. Thus we can assume a value of $\rho_e=10^{-4}$ $\Omega\cdot$m for any current densities of interest in this problem. ρ_e is also independent of electron density, except for a weak logarithmic dependence on its square root.

The total resistive energy loss for an acceleration time t is then

$$U_R=\int_{t_0}^{t_0+t}P\,dt=\frac{2B^2\delta_0}{\mu_0}\left[\left(1+\frac{t}{t_0}\right)^{1/2}-1\right] \tag{2}$$

Propulsive work done on the plasma during the stroke of length ℓ is

$$U_p=(B^2/2\mu_0)\ell \tag{3}$$

Also, for constant acceleration, $t=2\ell/v$, where $v=$ final velocity. These combine to give

$$\frac{U_R}{U_p}=\frac{4\delta_0}{\ell}\left[\left(1+\frac{t}{t_0}\right)^{1/2}-1\right] \tag{4}$$

$$=\frac{4\delta_0}{\ell}\left[\left(1+\frac{2\ell\rho_e}{\mu_0 v\delta_0^2}\right)^{1/2}-1\right] \tag{5}$$

The efficiency, as limited only by plasma resistive loss, is then

$$\eta_R=\frac{U_p}{U_p+U_R}=\frac{1}{1+(U_R/U_p)} \tag{6}$$

The extreme limiting cases of t/t_0 in Eq. (4) are of interest. If $t/t_0\ll 1$, we obtain, to first order,

$$\frac{U_R}{U_p}=\frac{4\delta_0}{\ell}\left(\frac{t}{2t_0}\right)=\frac{2\rho_e}{\mu_0 v\delta_0}=\frac{2}{R_m} \tag{7}$$

where R_m is the magnetic Reynolds number of the plasma.

Table 1 Effect of scale on thruster efficiency

ℓ, m	t/t_0	η_R
0.05	1.78	0.56
0.10	3.56	0.60
0.20	7.11	0.64
0.50	17.8	0.71

This is the case of a current sheet already so thick at formation that diffusion does not significantly thicken it during the stroke. Plasma velocity or specific impulse is a parameter here, but the scale size of the thruster is not.

For $t/t_0 \gg 1$,

$$\frac{U_R}{U_p} \simeq \frac{4\delta_0}{\ell}\left(\frac{t}{t_0}\right)^{1/2} = 4\sqrt{2}\left(\frac{\rho_e}{\mu_0 v \ell}\right)^{1/2} \tag{8}$$

In this instance, the current layer thickens significantly during the stroke and the plasma ring resistance drops. ℓ is now a parameter, such that a large accelerator improves efficiency.

Table 1 shows the effect of scale on efficiency for typical thruster parameters: $v = 2\times10^4$ m/s, $\delta_0 = 0.015$ m, and $\rho_e = 10^{-4}\ \Omega\cdot$m. Here, δ_0 and η are values usually achieved in these systems; they are not easily controllable.

While the above analysis is idealized it demonstrates that, *for the plasma parameters achievable in a pulsed inductive accelerator, efficiency, as limited by resistance loss, improves with size of the thruster.*

Numerical Simulation

We have simulated the pulsed inductive accelerator numerically with a model that represents the electrical parameters of the system quite accurately, but uses a highly idealized and approximate model of the plasma.[5]

Electrically, the thruster is modeled as a transformer of one turn in both primary and secondary. The primary is driven by a capacitor C, charged to voltage V_0; it contains parasitic inductance L_e and resistance R_e. The plasma secondary has resistance R_p. Figure 3 is an equivalent circuit of the system.

Both the coil and plasma are flat annuli of outer radius b and inner radius a. Each has inductance L_0 and they have a mutual inductance $M(Z)$, where Z is the axial separation between the two loops.

To within a few percent, the inductance L_0 is given by

$$L_0 = \mu_0 \frac{(a+b)}{2}\left[\ln\frac{b+a}{b-a} + 0.9\right] \tag{9}$$

and, empirically, we find that the mutual inductance is well approximated by

$$M = L_0 \exp(-Z/2Z_0) \tag{10}$$

If the primary and secondary currents are designated I_1 and I_2, an easily derived relation gives the force of repulsion between these currents

$$F_z = -I_1 I_2 \frac{\partial M}{\partial Z} = \frac{I_1 I_2 L_0}{2Z_0}\exp(-Z/2Z_0) \tag{11}$$

Then Newton's law couples the electrical and mechanical systems

$$\frac{\mathrm{d}}{\mathrm{d}t}\left(m\frac{\mathrm{d}Z}{\mathrm{d}t}\right) = \frac{I_1 I_2 L_0}{2Z_0}\exp(-Z/2Z_0) \tag{12}$$

The simplest representation of the plasma is that of a thin sheet of fixed mass m and assigned resistance R_p. We may use

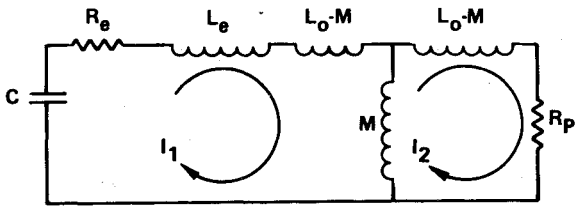

Fig. 3 Accelerator equivalent circuit.

it to solve the coupled electromechanical equations and obtain a plasma trajectory and accelerator energy efficiency. Such a grossly simplified model is not very useful, however, because it neglects the two important effects mentioned earlier as being major determinants of efficiency, i.e., the variable plasma loop resistance and "snowplow" losses associated with nonuniform acceleration of the total mass.

Accordingly, we have adopted a plasma model that incorporates both of these effects. We assume

1) The total injected mass m_0 is distributed uniformly over the annular coil in a layer of thickness δZ. While the current sheet moves outward through this interval, the total force on it is

$$F_z = \rho_m\left[Z\frac{\mathrm{d}^2Z}{\mathrm{d}t^2} + \left(\frac{\mathrm{d}Z}{\mathrm{d}t}\right)^2\right] \tag{13}$$

while, for $Z > \delta Z$

$$F_z = m_0\frac{\mathrm{d}^2Z}{\mathrm{d}t^2} \tag{14}$$

and we have passed from initial snowplow acceleration to slug model acceleration. In Eq. (13), $\rho_m = m_0/\delta Z$ is the initial axial gas density (in kg/m).

2) At $t = 0$, we must assume a finite plasma mass as well as an initial current thickness δ_0. For simplicity, we start with $m = \rho_m\delta_0$, where δ_0 is arbitrarily assigned (we rely on experimental experience for approximate values). Plasma loop resistance is then

$$R_p = \frac{\pi(b+a)}{(b-a)}\left(\frac{\rho_e}{\delta}\right) \tag{15}$$

where, as shown earlier,

$$\delta = \sqrt{\frac{\mu_0\rho_e}{t+t_0}}$$

and

$$t_0 = \mu_0\rho_e/\delta_0^2$$

This model was used for initial estimates of attainable efficiency as a function of scale size of the thrusters. Initial results were encouraging in two respects. First, the efficiency actually attained in two earlier experiments with 8 and 12 in. coils was in fairly good agreement with the computation. Second, the computation predicted a substantial improvement in efficiency with size, indicating that one might expect an efficiency of 60% for a 2 m coil and 5000 s I_{sp}. We were thus encouraged to build the 1 m thruster described in this paper.

Detailed discussion of the computational results will be deferred to a later section, where a meaningful comparison with experimental results can be made.

Experiment

Coil Design

The accelerator used for these experiments consists of a flat annular coil made of 36 one-turn spirals of 1.0×5.4 mm Litz ribbon conductors, embedded in a Lucite base plate, and

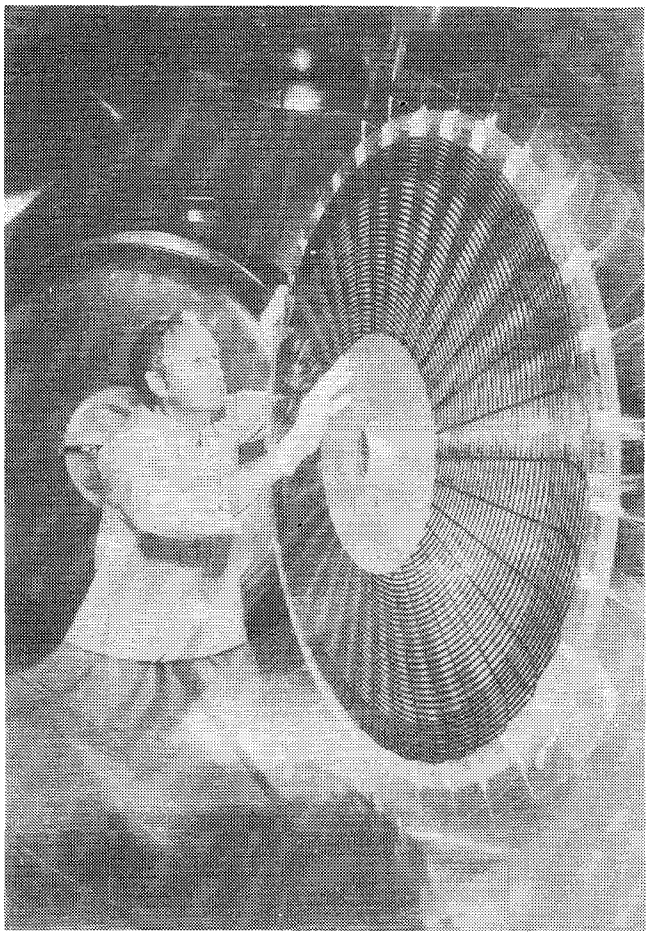

Fig. 4 Thruster coil in vacuum chamber.

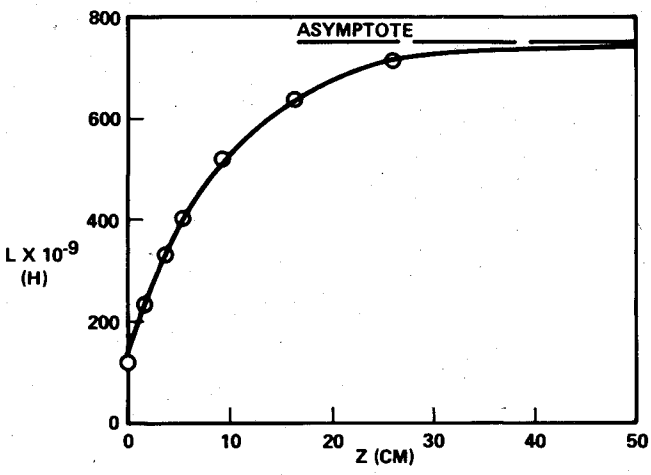

Fig. 5 Circuit inductance vs current sheet position (measured in test chamber).

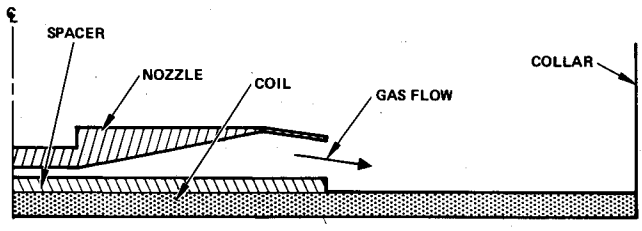

Fig. 6 Propellant injection nozzle geometry.

profiled in pitch to produce a constant azimuthal surface current density over most of the coil face. The coil has an outer diameter ($2b$) of 1.0 m and an inner diameter ($2a$) of 0.4 m (Fig. 4). As may be seen in the figure, the outer 6 cm of the coil is wound at a smaller pitch in order to locally increase current density and thus to compensate for the edge effect that would otherwise reduce plasma impulse in this region. Each of the 36 strands is connected near the coil center, to an RG-8 coaxial cable that leads out of the vacuum chamber to the energy storage bank. The bank has a capacitance of 20 μF and can be charged to 30 kV. A single spark gap switches the circuit. The work reported here was at a bank voltage of 20 kV or 4000 J energy. Figure 5 shows the total circuit inductance, including coil, cables, switch, and capacitors, as a function of the separation Z of a 1 m aluminum disk placed over the coil. At $Z=0$, the actual separation of plate and coil is 1.5 mm, the thickness of the Lucite insulating face. Thus, we assign a parasitic inductance ($L_e = L_{\text{ext}}$) of 0.120 μH to the circuit. Since this $L(z)$ measurement was done by actually firing the capacitor bank into the circuit and recording the "ring-down," the circuit resistance could also be deduced; we obtain $R_e = 7\times10^{-3}$ Ω. It may be noted that the simple expression of Eq. (9) gives $L_0 = 0.76$ μH for this coil, where the measured value, exclusive of L_e, is slightly over 0.70 μH.

Gas Valve and Nozzle

The correct initial deposition of the propellant gas over the face of the coil has been the most difficult technical problem in the development of this apparatus. The requirements on the filling are severe. First, the gas puff must be tight against the coil and thin. Any gap between the initial plasma breakdown and the coil constitutes a parasitic inductance and tends to decrease efficiency by reason of the $\Delta L/L_i$ criterion. If the layer is too thick, say comparable to Z_0 (the decoupling distance), snowplow losses will occur through most of the stroke, also reducing efficiency. Additionally, the entire mass of injected gas should achieve its optimum distribution simultaneously over all parts of the coil.

We employ a fast-opening solenoid valve, located on the axis of the coil and just above its plane, to empty the contents of a small, high-pressure plenum chamber into a radial supersonic nozzle, having a cylindrical aperture of 0.25 m radius and 0.025 m height. Measurements of gas distribution were made with a high-speed ionization gage that uses the exposed elements of CK5702 subminiature vacuum pentode. During these experiments, eight different nozzle configurations were tested, the best of which is shown in Fig. 6. The necessary condition that the first gas injected be reaching the outer coil edge when the last gas leaving the plenum has just reached the inner edge was met by adjustment of plenum volume and pressure. A typical combination is 6.5 atm of argon in a plenum of 1.86 cm^3 volume. Finally, it was found advantageous to confine the gas just moving past the outer edge of the coil by addition of a cylindrical Mylar collar of about 15 cm height. Figure 7 is a map of the axial distribution of density at five radii, 700 μs after valve opening. While pressure is decreasing toward the coil surface itself (probe size prevented a closer approach), it was nowhere so low as to prevent initial breakdown from occurring at the surface.

Diagnostics

We have determined thruster performance by a detailed mapping of $B_r(r, z)$ and $j_\theta(r, z)$ over that region of the r-z plane in which essentially all of the momentum transfer takes place. Integration of $F_z = j_\theta B_r$ over both space and time then yields the total impulse ΔI, from which one obtains

$$I_{sp} = \Delta I/mg \quad \text{and} \quad \eta = (\Delta I)^2/mCV_0^2$$

Data on one parameter for one spatial point are taken on each shot of the thruster. Thus, successful mapping demands excellent shot-to-shot reproducibility over runs of nearly 200 discharges.

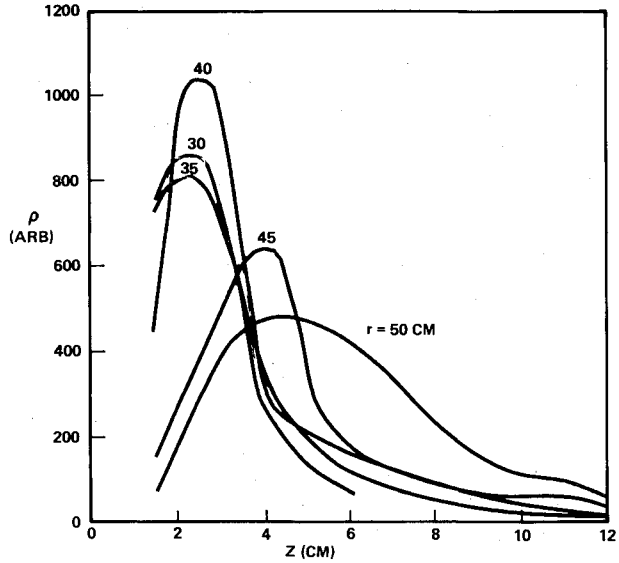

Fig. 7 Density distribution (1.86 cm^3 valve plenum, 700 μs delay).

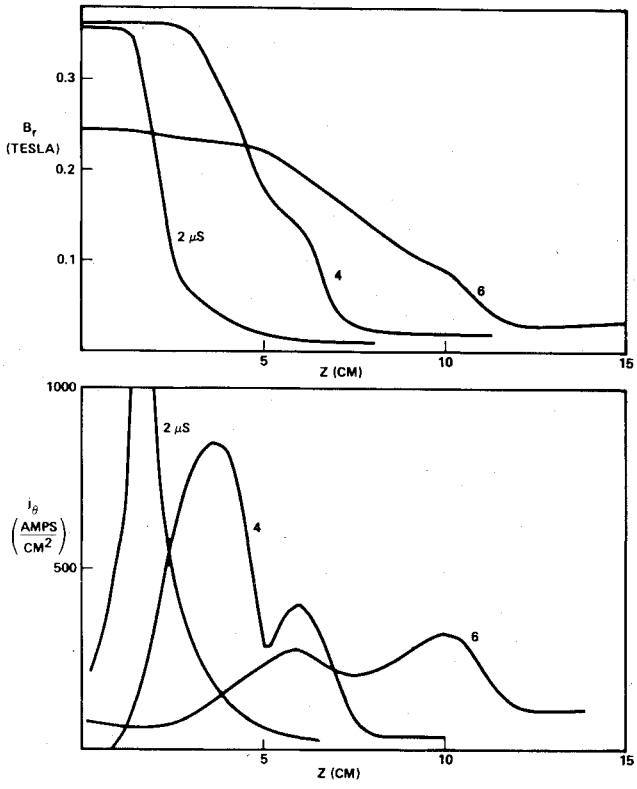

Fig. 8 Magnetic field and current density distributions at different times.

Each data run consists of B_r and j_θ probe records collected on a spatial matrix of 90 points in the r-z plane. Radial grid coordinates begin at $z=25$ cm, near the inner coil edge at $r=20$ cm, and continue every 5 cm to $r=50$ cm, the outer edge (six radial stations). Axial stations are spaced nonuniformly; the first six are at 5 mm intervals from $z=0.5$ to 3.0 cm. The next five are at 1.0 cm intervals to $z=8.0$ cm, and the last four are at 2.0 cm intervals to 16.0 cm. The reason for this arrangement is that the field and current distributions tend to be more compact and highly structured near the coil and more diffuse farther out; the greatest resolution is obtained in the region where most of the impulse is transferred.

The B_r probe is an open rectangular coil of five turns, extending 3 mm in the z direction and 1.0 cm along r. j_θ is measured by a toroidal "Rogowsky" coil extending 1 cm

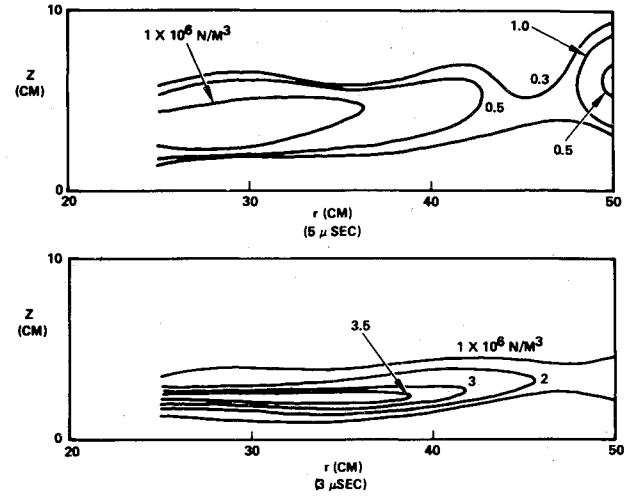

Fig. 9 Force density contours at 3 and 5 μs.

along z, with a window area of 1.3 cm^2. It has a novel balanced winding configuration which was found necessary in order to eliminate spurious electrostatic response.

Data Logging and Processing

Probe outputs are recorded in an 8-bit, 250-word digital transient recorder whose input includes an integration option. Each record is transferred, immediately subsequent to the shot, to a minicomputer where data on transient recorder gain, offset, and time step are appended to it, after which it is stored in a disk file. Each disk also stores programs that perform the computation of the force density distribution and the spatial and temporal integration of this force to arrive at the total impulse for the shot.

Experimental Results

The first conditions under which probe runs were made were the following:

$$\text{Gas plenum volume} = 1.86 \text{ cm}^3$$

$$\text{Gas plenum pressure} = 6.5 \text{ atm}$$

$$\text{Bank voltage} = 20 \text{ kV}$$

For the particular delay between gas valve opening and plasma acceleration that gave the best initial propellant distribution (700 μs), we estimate that 75% of the plenum fill was in place over the coil; thus the effective mass was 1.5×10^{-5} kg.

The total impulse for a shot obtained by spatial and temporal integration of j_θ and B_r at the 90 locations was found to be $\Delta I = 0.23$ N·s. This yields

$$I_{sp} = \Delta I/mg = 1540 \text{ s} \quad \text{and} \quad \eta = (\Delta I)^2/mCV_0^2 = 0.42$$

Examination of spatial distributions of j_θ, B_r, and force shows that the model of a single uniform sheet of plasma is too simple to represent the actual accelerator.

Figure 8 gives $B_r(z)$ and $j_\theta(z)$ at 2, 4, and 6 μs at a radius of 35 cm, approximately the midpoint of the coil. It is clear that the current layer thickens quite rapidly as it moves forward, a result that might be taken as indicative of high plasma resistivity. However, the thickening is evidently associated with a bifurcation in Z, rather than simple diffusion, since $j_\theta(z)$ becomes double-humped after 4 μs. The raw $j_\theta(t)$ records taken in the $z=4$-8 cm region display this double peak quite strongly. We are not prepared to explain this splitting at the present writing.

Figure 9 is a pair of contour maps of force density in the r-z plane at 3 and 5 μs. Qualitatively, these force distributions are about what one expects on simple grounds. However, one

anomaly appears here that repeats itself in all data taken with the present gas supply parameters: there is a pronounced dip in the force density in the neighborhood of $r=45$ cm. We associate this force dip with an actual dip in the surface mass density at this radius.

A particular departure of the real behavior from the simple model is the development of secondary current sheets upon reversal of the driving current. This is a common occurrence which is almost always observed in oscillating accelerators such as plasma guns and pinch devices. Normally, these secondary and tertiary sheets carry little mass and separate regions of equal and opposite field. They almost always originate at the insulator surface. Here, however, we observe the unusual instance of the second current sheet appearing well away from the coil surface. Figure 10 shows $j_\theta(z)$ at 9.0 μs for the six sampled radii. The negative peak in $j_\theta(z)$ at about $z=5$ cm is the first appearance of the second sheet. It has not propagated outward from the coil. This result plainly indicates that, at radii less than 35 cm, there is not enough residual plasma near the coil to support the current. At $r=40$-50 cm, some current flows at the coil as well as near $z=5$ cm.

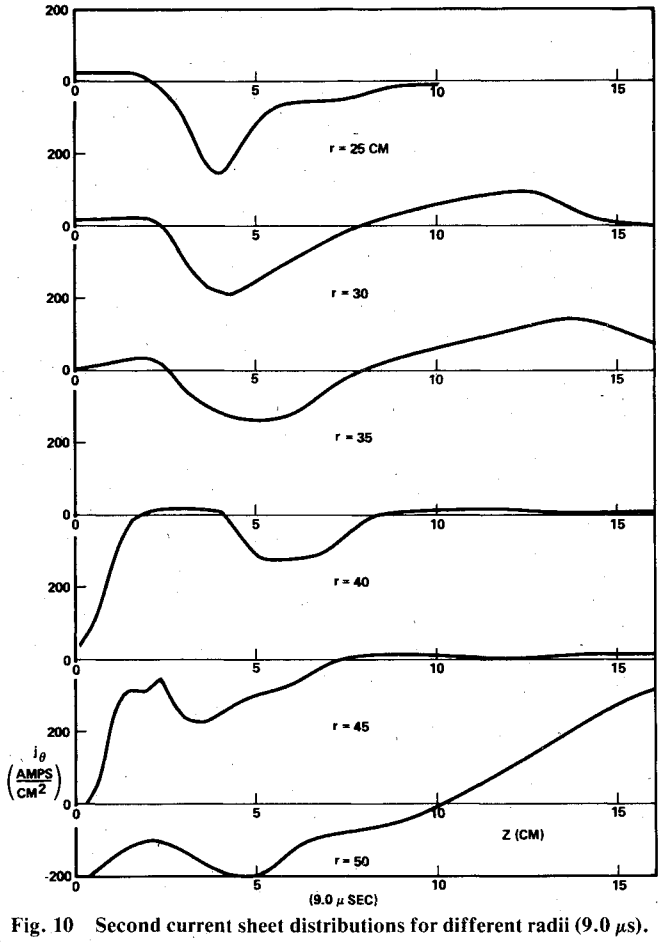

Fig. 10 Second current sheet distributions for different radii (9.0 μs).

Comparison with Computer Model

We may compare these experimental results with those of a computation of the model described earlier. To approximate the conditions of the experiment, we set

$$\delta Z \text{ (gas layer thickness)} = 0.04 \text{ m}$$

$$\delta_0 \text{ (initial current thickness)} = 0.02 \text{ m}$$

$$m_0 = 1.5 \times 10^{-5} \text{ kg}$$

$$\rho_e = 10^{-4}\ \Omega \cdot \text{m}$$

These yield a lower impulse than that actually observed, $\Delta I(\text{calc}) = 0.17$ N·s. For the same m_0 as used in the experiment, the I_{sp} and efficiency are correspondingly lower, i.e., 1160 s and 24%.

However, this computer model does not include the new current sheets that appear on the second and third half-cycles of current. We have, accordingly, modified the model to include these. On the basis of the observed dynamics of the second current sheet, we estimate that it accelerates about 15% of the injected mass, leaving about 5% for the third sheet. The results of computing this model under the other assumptions made above are that we obtain rather striking agreement between experiment and calculation. Both give an impulse of 0.23 N·s.

Figure 11 is a plot of two curves of the total force as a function of time, the solid curve derived from the j_θ and B_r probe data, and the dashed curve from the computer model. While the two forces agree almost exactly for the first 3 μs, the observed force is sustained at a somewhat higher level for the next interval until the current zero at 9 μs. During the second half-cycle, the computed force is higher.

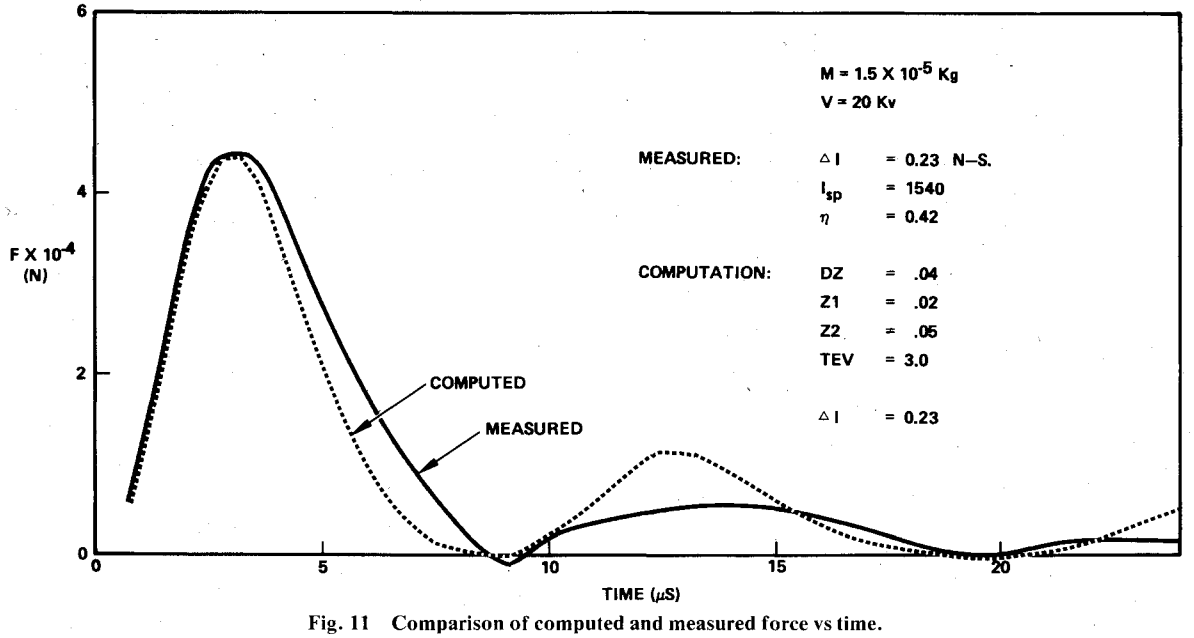

Fig. 11 Comparison of computed and measured force vs time.

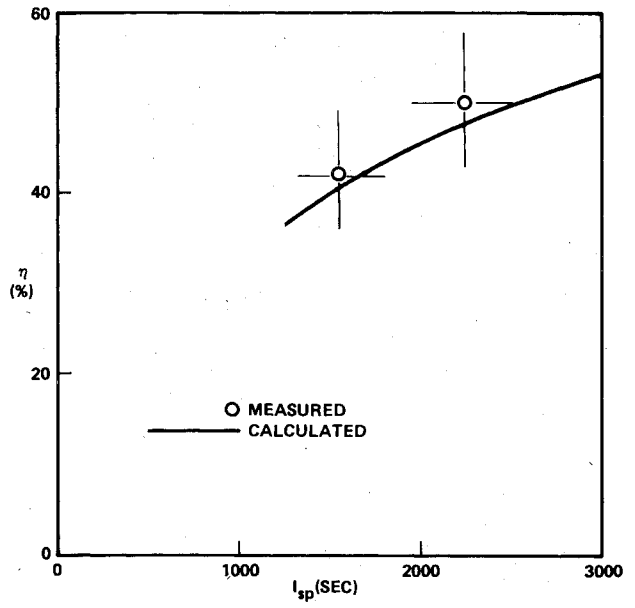

Fig. 12 Comparison of observed efficiency with theoretical model.

It is possible that these two curves could be brought into even closer agreement by some adjustment of parameters such as δ_0 and δZ. However, this hardly seems profitable in view of the crudeness of the model. We regard the principal usefulness of the comparison between experiment and computation in this instance to be as a plausible argument for the experimental results. Were there major errors in experimental assumptions, such as probe calibrations or adequacy of integration volume or time, it is extremely unlikely that agreement of this quality could be achieved.

We have examined one further operating point for which all conditions were maintained except the injected mass, which was reduced to 7.5×10^{-6} kg. The following results were obtained: $\Delta I = 0.182$ N·s, $I_{sp} = 2240$ s, and $\eta = 0.50$. The computation of this case also gave $\Delta I = 0.18$ N·s.

Comparison of Observed and Calculated Efficiencies

Our two experimental points are shown in Fig. 12 together with their probable errors. Also shown, as a solid curve, is the result of our numerical computations in which the assumptions on δ_0, δZ, and ρ_e are those given in the previous section and in which I_{sp} is varied by changing the accelerated mass.

A summary of the probable errors associated with measurement of the various parameters in this experiment is shown in Table 2.

Table 2 Experimental errors

Source	% Error	Derived quantity	% Error
B_r probe calibration	1	Impulse	8
j_θ probe calibration	3	Accelerated mass	11
Transient recorder gain	1	Specific impulse	14
Digitizing error in transient recorder	4	Efficiency	16
Transient recorder time base	4		
Gas pressure gage	5		
Injected mass fraction	10		
Force density numerical integration	5		

Discussion of Results

The derivation of η and I_{sp} from field measurements and gas distribution measurements involves several critical assumptions. First, the determination of total impulse through integration of $j_\theta B_r$ assumes azimuthal symmetry of the current and field system, since only one r-z plane is sampled. Earlier experiments[1,2] have confirmed this symmetry through both probing and photographic records, and photographs of the plasma from the 1 m predecessor to the present coil showed essentially perfect symmetry. Likewise, symmetry of the transient gas fill is assumed on the basis of the geometric symmetry of the injector.

The assumption that the actual gas load on the coil is equal to 75% of the original plenum fill is probably more open to question than are those concerning symmetry. Our assignment of a 10% error to this fraction is based on the estimated error in integrating the gas density curves (Fig. 7) at successive times in order to obtain the total fill mass as a function of time.

More serious is the possibility that the accelerated plasma contains a significant fraction of eroded Lucite from the coil faceplate. Erosion of insulators in pulsed devices is commonly observed and, were erosion occurring here, the actual accelerated mass would be greater than assumed, making η and I_{sp} correspondingly smaller for a given impulse. While such a contribution must be admitted as a possibility in this experiment, the data contain evidence that erosion is not a serious component. We argue as follows:

The two data points shown in Fig. 12 were taken at the same bank voltage, with the gas plenum pressure varied by a factor of two. If eroded Lucite were a major component of the plasma, this component should tend to be relatively independent of initial gas fill, depending more on bank energy. Observed impulse for the two cases would then tend to be the same. What we actually obtain for these two conditions are impulse values that not only have the correct ratio but also correct absolute values for nonerosive behavior of the discharge. We plan to replace the Lucite coil face with glass as the next step in the experiment, thus allowing a resolution of this question.

Conclusions

We have measured the impulse and efficiency of a 1 m pulsed inductive thruster and find that efficiencies as high as 50% are attainable. The fact that a single-current sheet model gives computed efficiency lower than that actually observed is not surprising if one considers that the formation of secondary and tertiary current sheets near the coil brings a larger fraction of the total mass acceleration into a more tightly coupled and, hence, more efficient configuration.

These results indicate that a thruster of this kind will be useful for high-thrust electric propulsion applications. A pulse repetition rate of 20/s will produce 0.45 kg (1 lb) of thrust at 1500 s I_{sp}.

References

[1] Dailey, C. L., "Pulsed Electromagnetic Thruster," AFRPL-TR-71-107, Dec. 1971.

[2] Dailey, C. L., Davis, H. A., and Hayworth, B. R., "Pulsed Plasma Propulsion Technology," AFRPL-TR-73-81, July 1973.

[3] Lovberg, R. H., Hayworth, B. R., and Gooding, T., "The Use of a Coaxial Gun for Plasma Propulsion," General Dynamics Convair Rept. AE62-0678, May 1962.

[4] Jahn, R., *The Physics of Electric Propulsion*, McGraw-Hill Book Co., New York, 1968, p. 269.

[5] Dailey, C. L. and Lovberg, R. H., "Large Diameter Inductive Plasma Thrusters," AIAA Paper 79-2093, Oct. 1979.